UNIVERSITY OF TWENTE.

Faculty of Science and Technology

Determining lipids of a multiple sclerosis axon using Coherent Anti-Stokes Raman Spectroscopy

Jos Nijhof

Individual research assignment

21 April 2022

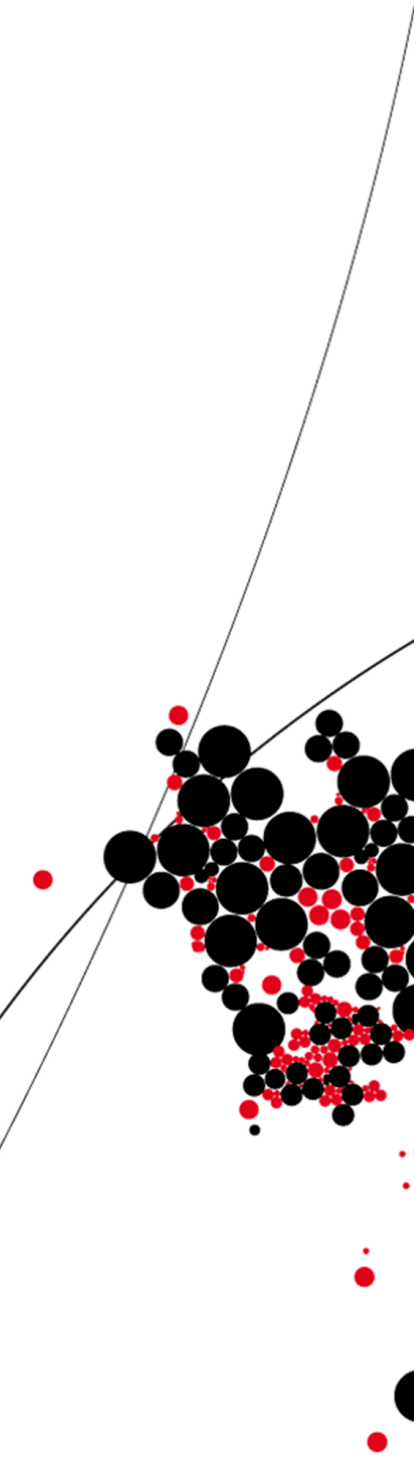

Supervisors:
dr. ir. H. Offerhaus,
dr. A. Luchicchi

Optical Sciences Group
Faculty of Science and Technology,
University of Twente
P.O. Box 217
7500 AE Enschede
The Netherlands

Preface

Before we dive into the material I would like to give a quick introduction as to why I researched this topic. The assignment was conducted as part of my masters curriculum into the education branch, Education and Communication in the Beta Sciences, specialising in the physics department. For this I was looking for an assignment that was best suited towards me. Having a bachelor in the medical sciences, Technical Medicine, I was looking for a physics assignment using a biological perspective. Optical Sciences proved (by chance!) to be the answer in this journey, which in collaboration with the Vrije University Medical Centra (VUMC) gave me the opportunity to combine these two facets.

Doing research is not always a straightforward line, there are many branching paths that lead to stagnation or backtracking. Little by little progress is made by sheer persistence. Nevertheless it is an important road to experience as it may not always be visible from the outside. Because I am going to be leading the example for the youth of today, it is important that their teachers are knowledgeable in the field of doing research. Especially because the field of physics can be quite complex and layered. I feel that I am now more capable of describing research and how it is done, and thus I feel that the purpose of the assignment has been realized.

Special thanks towards the technical staff (Jeroen Korterink) and everyone in the department that provided the working days with laughter and interesting conversation. Hopefully in the future I can strengthen the team with bright young minds!

Abstract

This paper has been conducted in support of research done at the Vrije Universiteit Medisch Centrum by dr. A.Luchicci to provide data for developing a new theory on why multiple sclerosis causes blisters in the axon-myeline connection. The research provides a possible pathway in which lipids break down due to glutamate neurotoxicity, resulting in a higher Ca^{2+} uptake in the myeline sheath.

A non-linear optical technology called Coherent Anti-Stokes Raman Spectroscopy has been used to image brain matter to look at lipid concentrations in or near axonal swellings. Multiple images have been condensed into a hyperspectral and analyzed for $C-H_2$ and $C-H_3$ lipid bonds, corresponding to the density of fatty acid lipids in the myeline sheath.

Results show a significant decrease ($P \approx 0.038$) of $C-H_2$ bonds between multiple sclerosis tissue swellings and normal-appearing axons, providing support for a theory that assigns lipid breakdown to the cause of swellings. Multiple Sclerosis swellings have also been compared with control swellings, which also show significant lower lipid concentration ($P \approx 0.030$), showing that multiple sclerosis progresses differently from normal swellings. $C-H_2$ has shown promis to be a useful marker in differentiating multiple sclerosis tissue from normal-appearing tissue.

A new setup is explored to acquire an even more specific signal using spontaneous Raman spectroscopy, but due time constraints was not finished.

Contents

Chapter 1

Introduction

1.1 Motivation

Multiple Sclerosis (MS) is a neurological disease that is occurring worldwide. Estimations from 2013 run up to 2.1 million cases of MS across the globe with no signs of slowing down [1]. A graphical overview can be seen in Figure 1.1. A high amount of countries (about 1 in 5) can not even provide any estimations because of a lack of MS organisations. Therefore MS still remains somewhat of a mystery in this highly scientific landscape. It stands to reason that more research in this field is highly necessary. This is where the field of physics and the field of biology can clasp hands and make great strides.

To get a better understanding of MS, we need to be able to look at it more clearly. Through microscopy or spectroscopy it is now possible to better quantify what we are looking at on a molecular scale. It is even possible to look at an atomic scale through the use of Atomic Force Microscopy [2]. This is possible in a static environment, but also on a high-speed time scale, resulting in a dynamic view of physiological processes. Optical sciences provide a way to use the special properties of light interacting with matter to further improve the knowledge about molecules and atoms. This paper thus focuses on using such properties to look at cells that are experiencing typical MS characteristics (to be further explained in chapter 2).

The research is conducted at the University of Twente, faculty of Science and Technology. The assignment is done in co-operation with dr. A. Luchicci to provide further data for his research of MS at the Vrije Universiteit Medisch Centrum (VUMC) [3]. He proposed to look at the lipids in cells damaged by MS to get a clear view of what is going on physiologically.

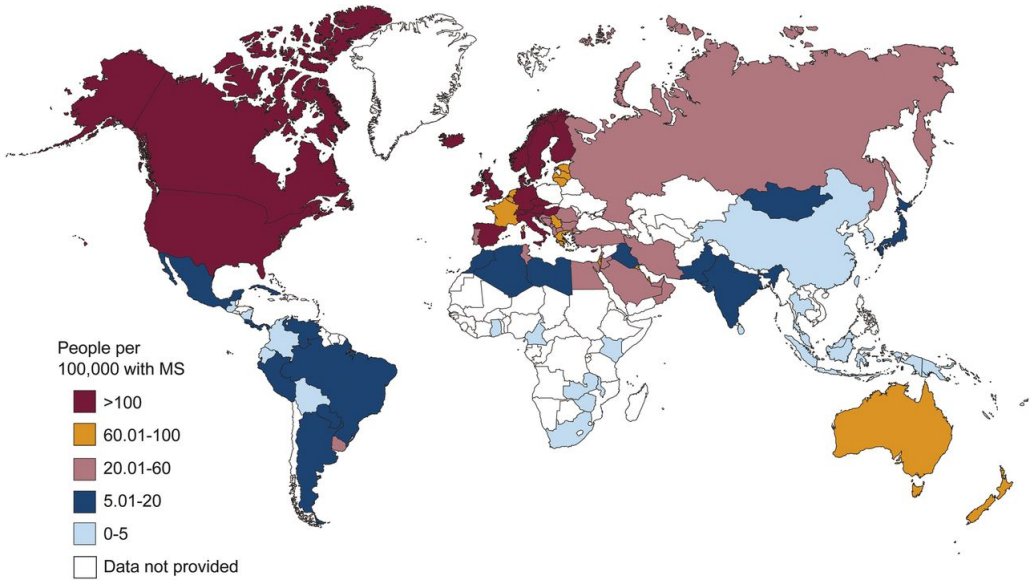

Figure 1.1: The prevalence of Multiple Sclerosis across the globe.
Source: ©`www.atlasofms.org`, MSIF 2013.

1.2 Research question

The research question is as follows: "How does the concentration of lipids in myeline damaged by Multiple Sclerosis change after the swelling of an axon?"

1.3 Report organization

The paper is divided into several chapters, of which you are reading the first right now. Chapter 2 contains all technical information which is required to understand the conducted research. Chapter 3 contains the method by which the experiment was performed including sample preparation and an overview of the scanning procedure. Chapter 4 shows the results acquired doing measurements using the aforementioned setup. Chapter 5 gives a conclusion. And finally, Chapter 6 contains a thorough recommendation of an alternate setup which could be used for further research.

Chapter 2

Theory

This chapter contains theory about both the physical and biological processes relevant to the research. First we take a look at linear optic effects and branch out towards the non-linear optics. The biological theory mainly describes multiple sclerosis (MS) and how it manifests.

2.1 Raman scattering

Light can interact with matter in various ways. The main pathways are transmission, absorption and scattering. In which a photon either passes through (in which case it actually does not interact with matter at all), gets absorbed or changes direction. The scattering in particular can either occur with the photon acquiring energy from the matter, or matter gaining energy from the incoming photon. Either way, energy is transferred and the incoming photon has a different energy from the outgoing photon and this process is called Raman scattering. A final third way of scattering is purely elastic, no energy is transferred. This is called Rayleigh scattering and can be seen by looking at the blue sky, which consists mainly of Rayleigh scattering of blue light while the other wavelengths get absorbed or are scattered less efficiently.

Why does this Raman scattering happen in the first place? To find this out we have to look at what light is at its most fundamental level. Light is a phenomenon of the Electro-Magnetic (EM) field. It propagates as a travelling wave and can be polarized in multiple fashions. This polarization is the key to Raman scattering. Electrons of matter can move and sway according to this polarization of light, which is expressed as follows:

$$P(t) = \epsilon_0[\chi^{(1)}E(t) + \chi^{(2)}E^2(t) + \chi^{(3)}E^3(t) + ...], \tag{2.1}$$

with $E(t)$ the electric field and its higher power orders and χ the susceptibility coefficient and its higher power orders. In the case of linear optics ($E(t)$ is small) all second

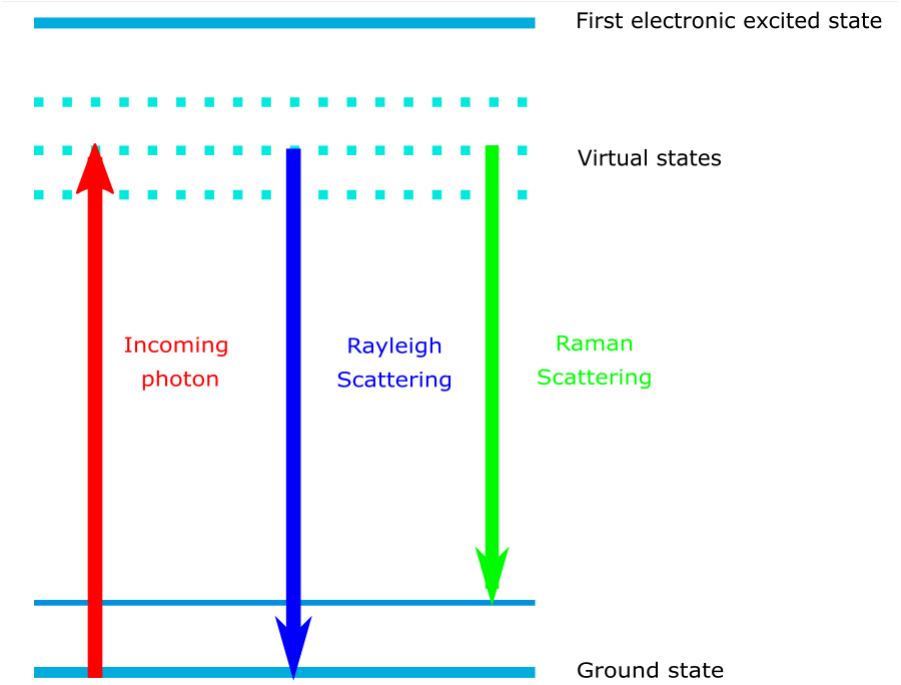

Figure 2.1: Energy level diagram showing Raman and Rayleigh scattering.

orders or higher are so small they are negligible. But as the intensity of the field rises the higher order terms are necessary to give a complete view of the polarization, to be further discussed in the next section.

Another way of looking at it is that the electrons energy level will rise because of the polarization of the electron. This higher energy state is very unstable and is therefore also called a virtual state. It is a state of a sort of complex bond between the light and the molecule and can not truly exist, thus the electron will release this energy as it falls down to the ground state and this released energy resides in the scattered photon, as we can see in figure (2.1).

The energy of a photon is directly related to its frequency according to $E_{ph} = h\omega$, with E_{ph} the energy of the photon, h the constant of Planck and ω the frequency of the photon. Thus the energy level of the virtual state will depend on the frequency of light that is shined upon the molecule, and will also influence the frequency of the scattered light. Raman scattering can always occur no matter what the frequency of the incoming light is, since it uses virtual states. This is very different from absorption, which uses real states in which the molecule can exist, and there are only discrete levels of these energies (quantized), thus also only discrete frequencies which can supply the energy for these states.

The aforementioned Rayleigh scattering occurs most of the time. With only one in 10^6 - 10^8 photons showing Raman scattering. This means that Raman scattering can be difficult to detect, and a high intensity of incoming photons is needed. A

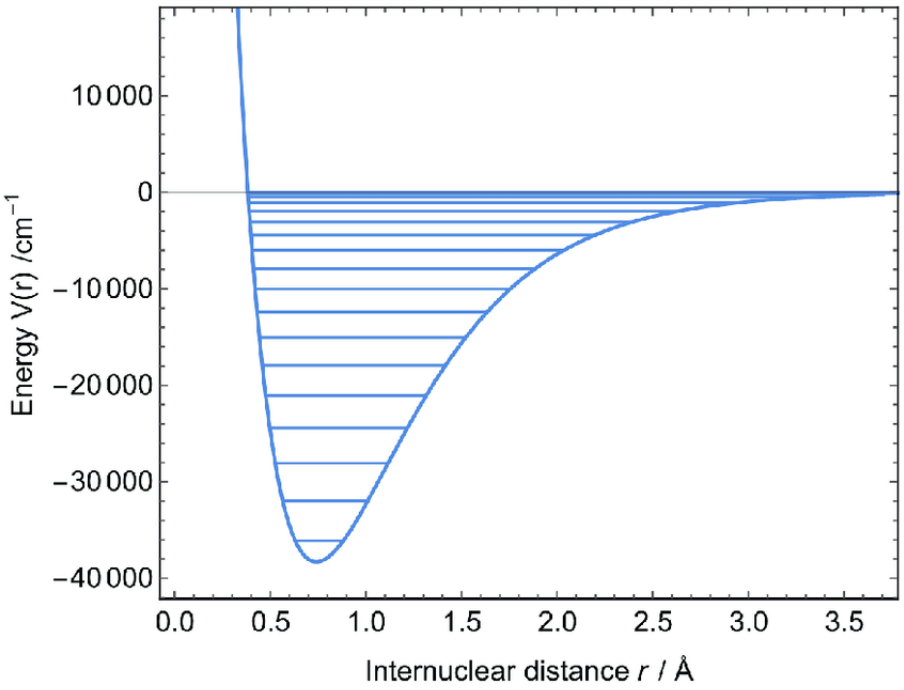

Figure 2.2: A Morse curve showing vibrational bands.
Source: `www.researchgate.net`

simple way to provide this amount of intensity can be done by a laser. Chapter 3 will show the experimental setup using such a laser. Laser light can be tuned in frequency and this can have advantages in acquiring the signal. Since there are other processes occurring during the interaction of light with matter we can make a better selection of which process to dim out and which process to enhance. For example, in our case we want more Raman scattering and less fluorescence. Fluorescence in this way competes with Raman scattering and we want to suppress it as much as possible. This usually means exciting the sample at higher frequencies. What does the Raman scattering then say about the molecule? The answer is simple: *vibrations*. Molecules have bonds between their atoms and these bonds can have a certain amount of energy. The morse curve in figure 2.2 shows the relation between this energy and the separation between nuclei. There are also bands of lines called vibrational levels. Thus a molecule can have multiple energy levels at ground state. When Raman scattering is occurring it can happen at the ground vibrational level but just as well at a higher excited vibrational level. However the energy of the scattered photon differs between these processes. Figure 2.3 shows that when a molecule at ground vibrational level shows Raman scattering, then the molecule will be in a final excited vibrational state. This process is called Stokes scattering. Likewise, when a molecule transfers energy to the outgoing photon it will go from an excited vibrational state to the ground vibrational state.

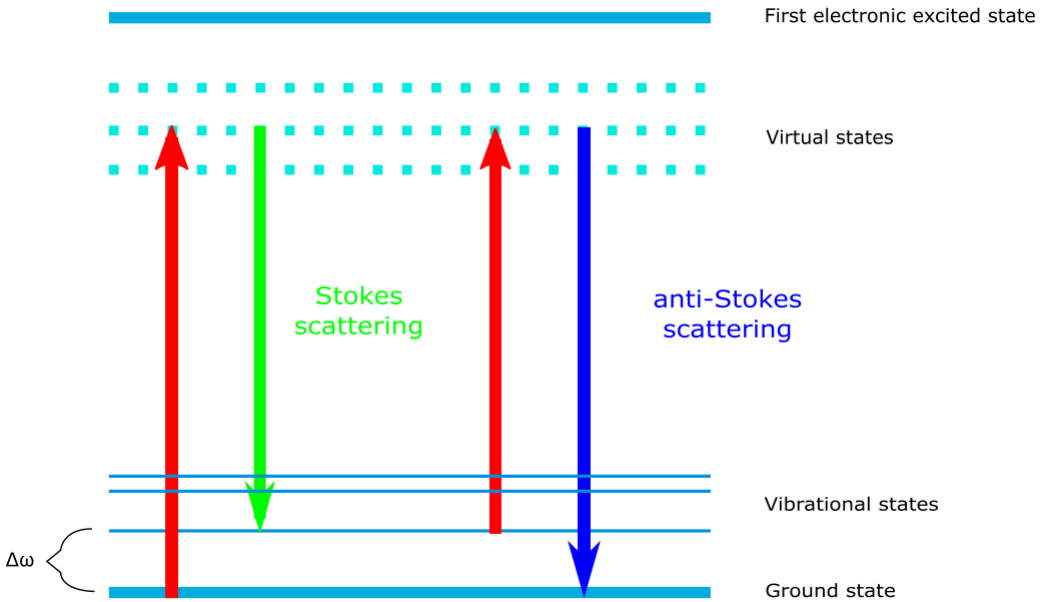

Figure 2.3: Energy level diagram of both Stokes and anti-Stoke effects, note the frequency difference in the bottom left.

Stokes scattering is more prevalent in normal room temperature conditions since most of the molecules are at ground level. Raman scatter can thus be used to measure these energy levels between the vibrations. The difference of the incoming frequency and the scattered frequency due to Raman can be determined by the following:

$$\Delta\omega[cm^{-1}] = \left(\frac{1}{\lambda_i[nm]} - \frac{1}{\lambda_s[nm]}\right) \times \frac{10^7[nm]}{[cm]}\,, \tag{2.2}$$

with $\Delta\omega$ the frequency difference in $[cm^{-1}]$, λ_i the wavelength of the incoming photon and λ_s the wavelength of the scattered photon. The $[cm^{-1}]$ notation is conventionally used in the spectroscopy field and represents the wavenumber. It is this wavenumber that signifies the vibration energy level. All bonds have a certain characteristic vibration energy level dependent upon the strength of the bond, and therefore it is possible identify molecules in samples. A quick side note to mention is that Raman scattering is mainly used to detect symmetric vibrations, because the symmetric bonds cause large polarization changes.

2.2 Coherent anti-Stokes Raman Spectroscopy

In the previous chapter we have looked at Raman scattering, a linear optical effect. This means that the strength of the Raman scattering signal scales linearly with the incoming light power. We have also seen that it heavily depends on the ability of light

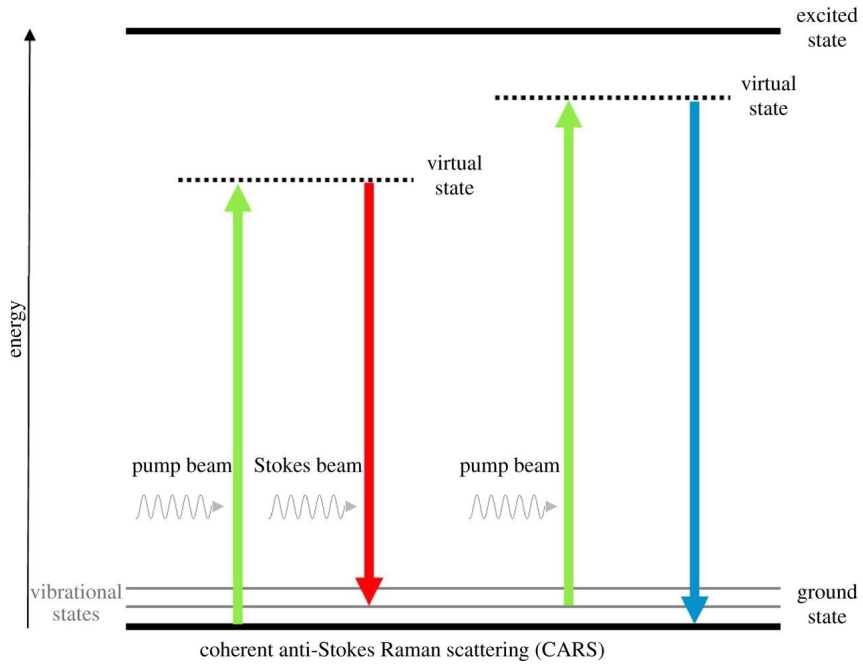

Figure 2.4: A figure showing how the pump beam (green) can be used in succession with a stimulated Stokes beam (red) to create the anti-stokes/CARS frequency(blue) [4]

to polarize molecules/electrons. In equation (2.1) we have seen that multiple higher order terms are necessary for a complete explanation. In non-linear optics these terms become relevant. It essentially means that multiple photons can hit matter at the same time, resulting in different effects that do not scale linearly with the intensity of the photons. We can use this to our advantage. Coherent anti-Stokes Raman Spectroscopy (CARS) uses a complex setup of multiple lasers, or in our case a laser which is able to create two different bundles of frequency, to excite matter with a high chance of multiple photons hitting the target at (nearly) the same time.

The following figure 2.4 shows how two photons can excite towards a higher energy state, and how three photons can create the CARS effect. These frequencies are called the pump frequency (ω_p), Stokes frequency (ω_s) and the anti-Stokes frequency (ω_{as}). The pump frequency can be used twice (from the same laser source) to create the anti-Stokes, which results in $\omega_{as} = 2\omega_p - \omega_s$. A molecule which is in resonance with the beating frequency (ω_p - ω_s) can be excited to a vibrationally excited state in this way. The energy that characterizes the vibration can be calculated with (2.3) using the anti-Stokes wavelength as the scattered photon wavelength.

This method has the benefit of creating a much larger signal than is acquired with normal spontaneous Raman scattering (up to nine orders of magnitude) [5]. The intensity of the signal does not scale linearly with the intensity of the pump but like

this:

$$I_{CARS} \propto I_{pump}^2 I_{Stokes}. \tag{2.3}$$

This is exactly the reason why it is possible to do CARS imaging at a relative high speed. To realise this, a laser is needed in which it is possible to fine-tune the frequency output to directly excite the targeted vibrational state. This can be done through an optical parametric oscillator (OPO). An OPO uses an optical resonator with a non-linear crystal, which combined can create two new frequencies from a single input frequency. Thus it is possible to fine-tune your pump frequency and create a strong signal at which the molecules resonate.

However, there are also electronic motions which contribute to this signal, called the non-resonant background signal. This arises from the third-order polarization term in equation (2.1), where the susceptibility $\chi^{(3)}$ has a resonant component, a non-resonant component and a mixing component like so:

$$(\chi^{(3)})^2 = (\chi_R^{(3)})^2 + (\chi_{NR}^{(3)})^2 + 2\chi_{NR}^{(3)} Re[\chi_R^{(3)}]. \tag{2.4}$$

The non-resonant component is relatively constant so it merely down-shifts the spectrum. The final mixing term will interfere such that the peak of the CARS signal will shift to the lower frequencies, while the higher frequencies will be suppressed. Because this term overlaps with the CARS signal, it is not possible to filter this using typical optical filters. All in all, CARS remains to be a highly effective tool to localize targeted matter due to its high signal acquisition and low interference with fluorescence, which is overabundant in biological matter.

2.3 Multiple sclerosis

Multiple sclerosis (MS) is classified as a demyelinating disease [6]. It affects the central nervous system, in which it disrupt all functionalities of myeline. Myeline is a sheath around nervous cells, called axons, which mainly consists of lipids. The main function of axons are to propagate electrochemical signals called action potentials, while lipids are mainly found in membrane structures and posses the ability to isolate matter from its surrounding or create layers [7]. The larger an axon is in diameter, the faster it can signal the action potentials. The function of myeline is thus to facilitate a quick action potential pathway while the axon remains small in diameter. They allow an axon to skip its regenerative cycle from one node to the next, instead of gradually spreading it down the whole of the axon. This effect is called saltatory conduction and crucial for optimal action potential propagation. Central myeline is made by oligodendrocytes, while peripheral myeline is constructed by Schwann cells. The border between central and peripheral nerves is around the exit of the brain stem or the spinal chord. If myeline were to break down, as happens in MS, there could be a great number of problems in

signal propagation. High-frequency signals are cut off, complete blockage may occur and axons can spontaneously generate their own action potentials or communicate with adjecent demyelinated axons, inducing crosstalk.

MS is defined by the plaques which accumulates in the brain, around 2-10 mm in size [8]. They are visible as darkened spots in the white matter, although it can breach into the gray matter. Any part of the central nervous system can be affected but a preference remains for the optic nerves, optic chiasm and paraventricular white matter. The plaque manifests as the loss of myelin with an abundance of lymphocytes (white blood cells) and macrophages that attempt to recover any damage. To this day it is unknown if this immune response is the reason why the myeline degrades (auto-immune) or if it is the immune system reacting to a toxic event. This toxic event can occur due to a high excitatory glutamate, which acts as a neurotransmittor. Active MS lesions show elevated levels of glutamate and this could contribute to an excitotoxic mechanism that leads to neurodegeneration [9]. It can occur in patterns as relapsing and remitting (RRMS $\approx 80-90\%$) or in a more progressive nature (primary and secundary progressive, PPMS, SPMS $\approx 10-20\%$). The relapses occur mostly due to exacerbations caused by inflammation . A remission is thus possible after the inflammation subsides.

2.4 Axonal swelling

There are numerous ways for an axon to be damaged, some examples were provided in the last paragraph. But the results are nearly always similar. The pathway between axon and myeline is disturbed, resulting in a detachment of the myeline sheath, thus providing space for extracellular fluids to increase, leading to a swelling. The particular cause of these swellings in MS are unknown at this moment, but there are studies showing possible pathways. One of such pathways is shown in figure 2.4. We are going to divide this up in steps as follows:

(1),(2) and (3) are instigation effects.
(3),(4)and (5) are regulation effects due to the instigation.
(7),(8) and (9) are the result of the regulation effects.

The instigation effects can vary and are of a particular nature in this case.

1. Na^+ outside the cell transfers into the cell due to elongation of the axon at a node (or other morphological changes). They can enter through Na^+ channels or active voltage gates. Another process described at (6) can result in ion uptake (1b).

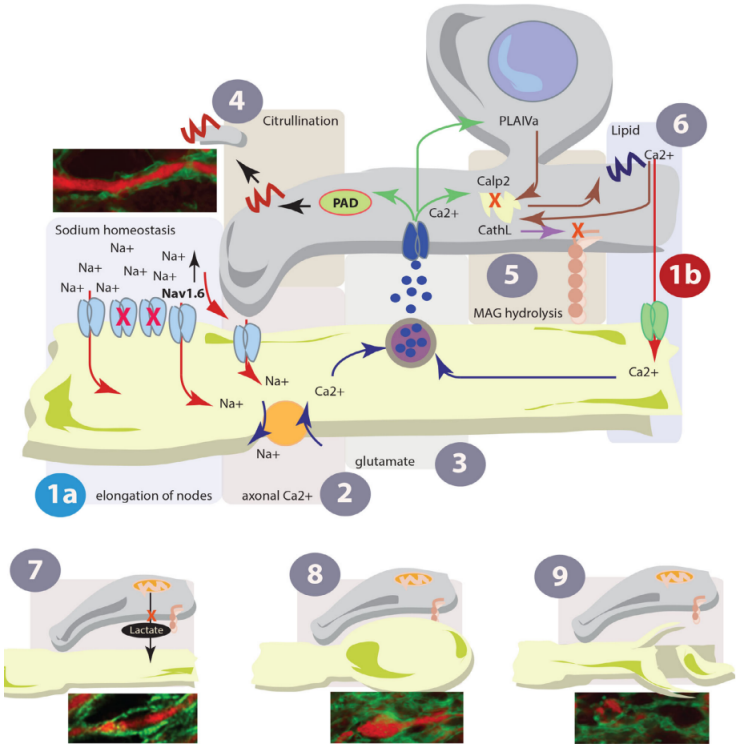

Figure 2.5: Possible pathway of axonal swelling and degeneration, with (7),(8) and (9) showing a time-lapse of an axon swelling. Showing the axon in a red colour and the myeline sheath in green. [3]

2. Higher uptake causes stimulation of activity in the Sodium-Calcium channels, resulting in lowering the concentration of Na^+ and an increase of Ca^{2+} in the axon.

3. Glutamate acts as a neurotransmittor to transport the Ca^{2+} from the axon to the myeline. The a higher concentration of axonal Ca^{2+} leads to a higher uptake of Ca^{2+} in the myeline.

   The higher Ca^{2+} uptake will be used to make certain processes happen within the myeline. This is the regulatory part of the chain and will happen regardless of how the Ca^{2+} uptake was achieved.

4. Ca^{2+} facilitates the enzyme peptidyl arginine deiminase (PAD) which can break down arginine into citrulline. Arginine is found in multiple myeline proteins and thus this proces will hinder processes which use these proteins. The resulting citrullination might act as a starting signal for the adaptive immune response and thus will result in inflammation.

5. Ca^{2+}initiates a cascade resulting in the hydrolysis of myline associated glycoprotein (MAG) which are paramount for structurel adherence and tethering of the myeline to the axon. This breakdown ultimately is the cause for demyelisation.

6. Another effect of the cascade described in (5) is the altering of the lipid structure inside myelin. Resulting in biochemical changes which can reduce the potency of the membrane to act as a barrier. Thus Ca^{2+} can leak into the axon (1b), furthermore increasing the activity of glutamate (3).

   Once MAG is broken down into its degenerate state the myeline will release itself from the axon, thus resulting in impaired function of conducting a signal.

7. The myeline sheet detaches itself from the axon, causing a blister-like structure to exist. During this process the lactate-dependant signal from the myeline to the axon is severed. The axon is dependent on this signal for the working of the mitochondria, which provides the cells the energy to maintain or grow. Therefore the axon grows into a hypoxic state.

8. Due to hypoxia the axon swells up.

9. In the end the axon will degenerate because it can not maintain its cells, and thus loses it's conducting properties.

This paper will focus on part (6), the lipids. With a change (reduction) in lipids being a measurable component, we can look at MS tissue and compare them with normal tissue. The aim is not to look at the cause (the instigation) but to see the

lipids as a kind of biomarker as a precursor to lesions. A reduction in lipids would provide more support for the "inside-out" theory.

Chapter 3

Method

3.1 Sample preparation

The samples are acquired after thorough obduction at the Antoni van Leeuwenhoek hospital. Small cubes of brain matter are sliced near lesions of the corpus callosum and just outside this area (extra corpus callosum). These are fixated in 4% formalide for 24 hours or longer. When this is done, the samples transfer to a solution of 5 - 10% sucrose and phosphate buffered saline (PBS) to maintain pH and osmotic balance. This is separated again later using precipitation techniques, after which the small cubes are frozen in at -30° Celcius and sectioned in a Leica Biosystems^{TM} cryostat, wherein the cubes are sliced in coupes of 200 μm. Finially the coupes are put in FluoroDish Cell Culture^{TM} dishes with PBS and 0.002 sodium azide [10]). The dishes have a coverslip thickness of 0.17 mm and a refractive index of 1.525 which allows magnification up to 100 times.

When using the samples in the microscope it is of the utmost importance that they are pressed towards the bottom of the dish. Failure to do so will result in difficulty focusing on the sample because the sample will be free to float and thus the focus will drift. Small blocks of PDMS are inserted on top of the sample to rectify this problem. Because the sample is illuminated from the bottom and detected in the epi-direction, it does not interfere with the acquired signal at all. Also the formaline has been shown to not interfere with the acquired CARS signal.

3.2 Experimental setup

Due to CARS being a non-linear optical method, we require a highly intensive beam of light to illuminate the sample. This is realised by the NKT aeroPULSE fiber laser, which can generate pulses up to 6 ps at a repetition rate of 80 MHz. The CARS requires two ω_p frequencies and a single ω_s frequency. This can all be accomplished with this single laser source. The fundamental laser wavelength is 1032 nm and part

of this is used as the ω_s frequency. The other part is doubled in frequency, and thus halved in wavelength to 516 nm, using a second harmonic generation crystal. This beam is guided into a Levant APE germany^{TM} optical parametric oscillator (OPO), where the beam is split into two parts $\omega_{beam} = \omega_{signal} + \omega_{idler}$. We direct the idler towards a beam blocker, and use the ω_{signal} as our ω_p. This frequency can be tuned to generate the CARS signal range over which we measure our sample. It is possible to modulate the ω_s using an acoustic optic modulator (AOM) coupled to a function generator if necessary, it was not used in this research.

It is important that the ω_p and the ω_s are correctly aligned, spatially and temporally. thus a pathway delay stage is introduced to realise this. It is also important to monitor the power of both the ω_p and the ω_s. Using a low reflectance mirror we can direct a small part of the beam into a spectrometer (Ocean Optics^{TM} HR200, Netherlands) which is coupled to a computer for readout. This way we can make sure that both beams are optimized in intensity and that we have tuned for the right frequency. The OPO can be adjusted in cavity length, temperature and lyott position to fine-tune this process. Finally the beams come together using a dichroic mirror and together they enter the scanning box.

Scanning is done by a moving set of galvometer mirrors, before the light enters the microscope. In the microscope itself the beams pass a filter wheel which is adjustable. For our experiment we used a FF705 dichroic together with a 641/75 filter. This ensures that the wavelength used to excite the sample is filtered out and the CARS signal is reflected out of the microscope towards a detector. A 60x 1.2 NA Olympus UplanSApo^{TM} water immersion objective is used to focus the light on the sample, after which the light scatters and a CARS signal is created in the epi-direction. The detector of use is a photomultiplying tube (PMT), a Hamamatsu^{TM} R3896. The PMT is connected to a computer for readout and the Ocean Optics Fluoview^{TM} software tool can thus create an image out of the PMT values.The final image is generated through the values that the PMT detector acquired during scanning of the sample. The resolution of the frame is 512 x 512 pixels, with a spacial resolution of ≈ 0.9 μm /pixel. Axons can be as thin as 0.1 μm [11] thus a high resolution is required to look correctly at swellings of an axon. A full figure containing the setup is shown in Figure 3.1 [12]

3.3 Hyperspectral

Using Labview^{TM}, a programming software tool, it is possible to let the setup scan over multiple wavenumbers. In this tool the Fluoview software can communicate with the Labview program to scan at certain intervals, with each interval using a different wavenumber. Thus you can scan a sample in area but also spectrally over a range

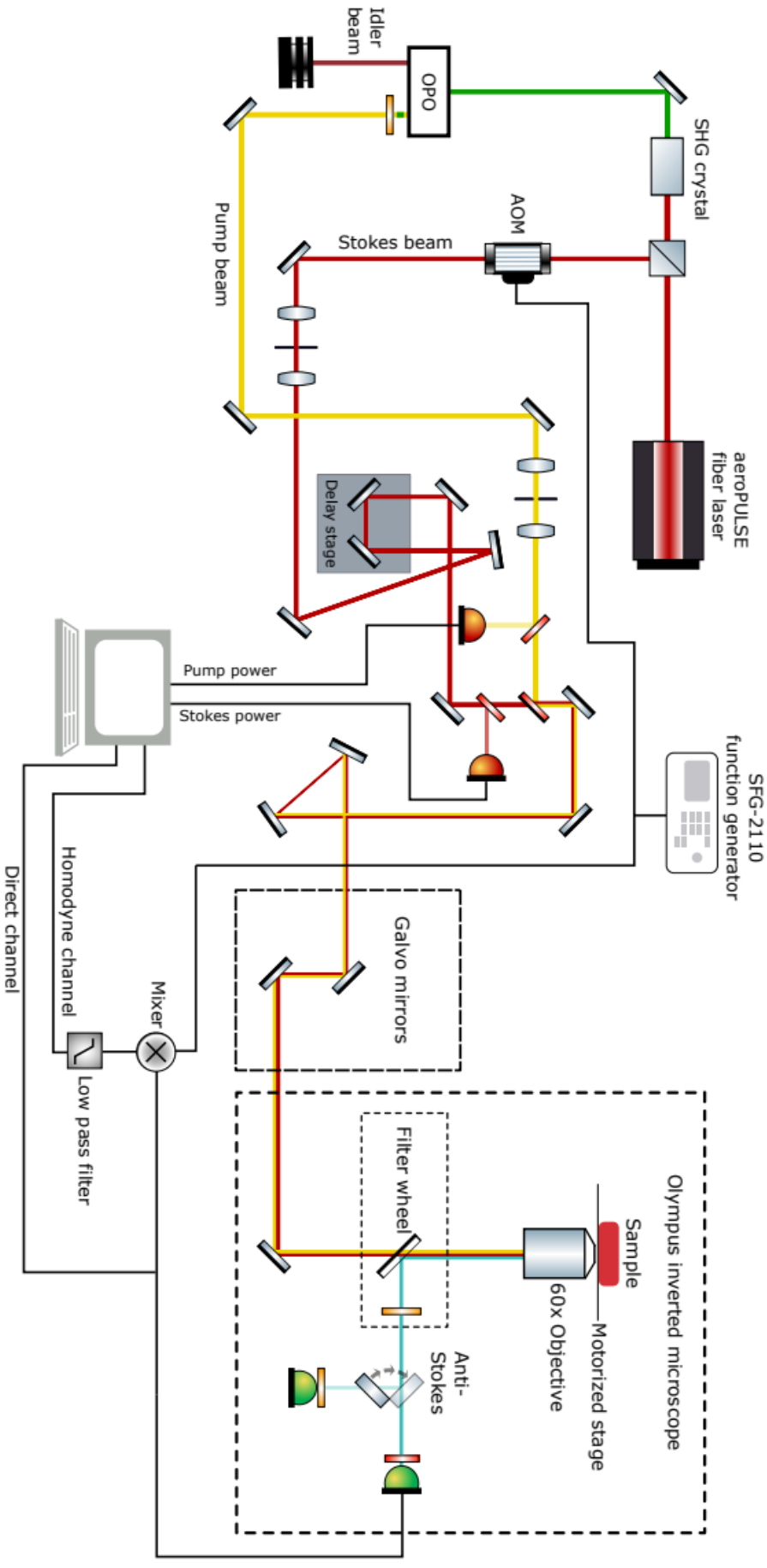

Figure 3.1: Experimental CARS setup.

Molecular binding	Wavenumber
$C - H_2$	2848 cm^{-1}
$C - H_3$	2934 cm^{-1}
H_2O	3140 cm^{-1}

Table 3.1: Wavenumbers of molecular bindings encountered in swellings of axons.

of wavelengths. This set of data is called a hypercube, and can be analyzed using Matlab™. The x and y components represent the spatial coordinates in the image and the z component is the specific CARS wavenumber at which the image was scanned. The amount of steps needed to complete this range can be tuned, but is chosen to be 144 frames for these sample measurements.

It is important to let the scan speed be slow enough for the OPO to adjust its values, the temperature in particular. Furthermore, changing the OPO values will have an affect on the power, which needs to be corrected for. This will be further discussed in Chapter 4.

The important wavenumbers we want to look at are visible in table 3.1. Myeline contains a lot of $C-H_2$ and $C-H_3$ bindings. Thus we suspect that the range resonating with these bindings are going to be of interest, as a difference in concentration of these bindings may contribute to the swelling of an axon. The range chosen to create a hyperspectral is 2700 - 3200 cm^{-1}.

To summarize the workflow of a hyperspectral scan:

1. Prepare the sample, making sure that the sample is sufficiently pressed against the bottom of the dish.

2. Set the wavenumber range over which to scan the sample accordingly, in this case 2700 - 3200 cm^{-1}.

3. Find the focus spot using the microscope. Preferably a substantial amount of axon swellings can be seen in one frame. Once found, let the microscope wait for a trigger to start the hyperspectral.

4. Set the initial OPO values right (piezo actuator to determine the stokes frequency, lyott filter and temperature) and give the microscope the trigger to begin scanning. The microscope scans one frame and then waits for another trigger.

5. Each next frame introduces a small delay to let the OPO values change accordingly, and then gives another trigger for the next scan. Repeat till all 144 frames are scanned.

6. All data that is detected is collected and can be read out in various programs. The program of choice is Matlab™.

Chapter 4

Data Analysis

4.1 Image creation and calibration

When a measurement is done, it can be loaded into Matlab^{TM}. The PMT values give the intensity values of each pixel in a range of 144 frames. Thus we can create a stacked image out of these values. As shown before in equation 2.3, the intensity of the CARS signal is higly dependent on the intensity of the stokes and pump beam. The power of the pump beam (controlled by the OPO) is not constant during the hyperspectral sweep and thus we need to compensate for this. The total power is first normalized, with the highest obtained power set to 1. Then all intensity values are divided among this normalization to offset this power inequality. From this signal another subtraction is done because of background noise (the value of the PMT during no active measurements), from other research using the same setup it is found to be 50mV [12]. The PMT also shows a variation in gain over the wavelength of the incoming photons. We assume since we used the same setup to create all images, this will not give a problem between comparing spectra, as all spectra have this same gain factor. However, this makes comparison with other spectra generated in different setups difficult. A final consideration is the voltage/gain curve of the PMT but since the voltage was held constant of the PMT (at the value 666V), it does not pose a problem for signal compensation. At last, the final signal is converted to a grayscale with a max value of 4095 (due to a depth of 12 bit pixels). From this signal an image is created.

4.2 Image analysis

The image in question can be analysed using a tool to select an area of pixels and combine their value. The signal is then averaged over all selected pixels. A single pixel can also be selected but this results in a very noisy graph. In general we can say that more pixels selected will result in a smoother graph. However, selecting too many

pixels will result in a loss of interpretation, as we do not know if we still are looking at the myeline or surrounding tissue. It is possible to create a zoomed in picture (62 times magnification) but this comes at a cost of lower signal since the sample can be easily burned at this magnification. Thus a balance has to be found.

The final data is an array of numbers containing the averaged signal over the selected pixels on each frame. Each frame corresponds with a wavenumber, thus it is possible to make a plot of the wavenumber and the signal. The result is a spectrograph containing peaks at the resonating vibrations. These peaks can then be analysed and compared with other samples. Since the signal is higher at points with more vibrating bonds, the relative concentration of bonds can roughly be estimated. The intensity of the signal is of an arbitrary value, thus the concentration is arbitrary too. But it is still possible to make a good comparison with other samples to determine if the concentration has changed.

Chapter 5

Results

5.1 Hyperspectral results

Hyperspectral scans have been done on 3 MS samples and 5 control samples. Not all samples were scanned on the same magnification due to burning the sample at high intensity. Figure 5.1a is an example of a sample which shows a large amount of axons in brain matter. Multiple areas could be selected and from these a spectral graph was made, see figure 5.1b. We can see that the sample shows peaks at the aforementioned wavelengths, namely 2848 cm^{-1}, 2934 cm^{-1} and 3140 cm^{-1} (shown in table 3.1).

Thus a hyperspectra could be made within a sample, but we are interested in how samples differ from one another. Therefore all hyperspectra of all the samples were grouped together, which you can see in figure 5.2. A swelling contains the main region of significant axon dilation, whereby pre/post swelling contain the proximal/distal regions positioned relative to the the swelling. Finially normal-appearing white matter was scanned in the control group for comparison.

We can zoom in further on the regions of interest, namely the $C-H_2$ bond and the $C-H_3$ bond. The results are presented in figure 5.3. You can see a clear reduction in the $C-H_2$ bond of MS samples versus the control samples. Note that normal-appearing matter is the same in swelling and pre/post swelling, as they classify as both at the same time for easier comparison. A similar but reduced reduction can be seen in the $C-H_3$ bond. Another point of interest is the broad peak around 3100 cm^{-1} which suggests a higher concentration of water in swellings.

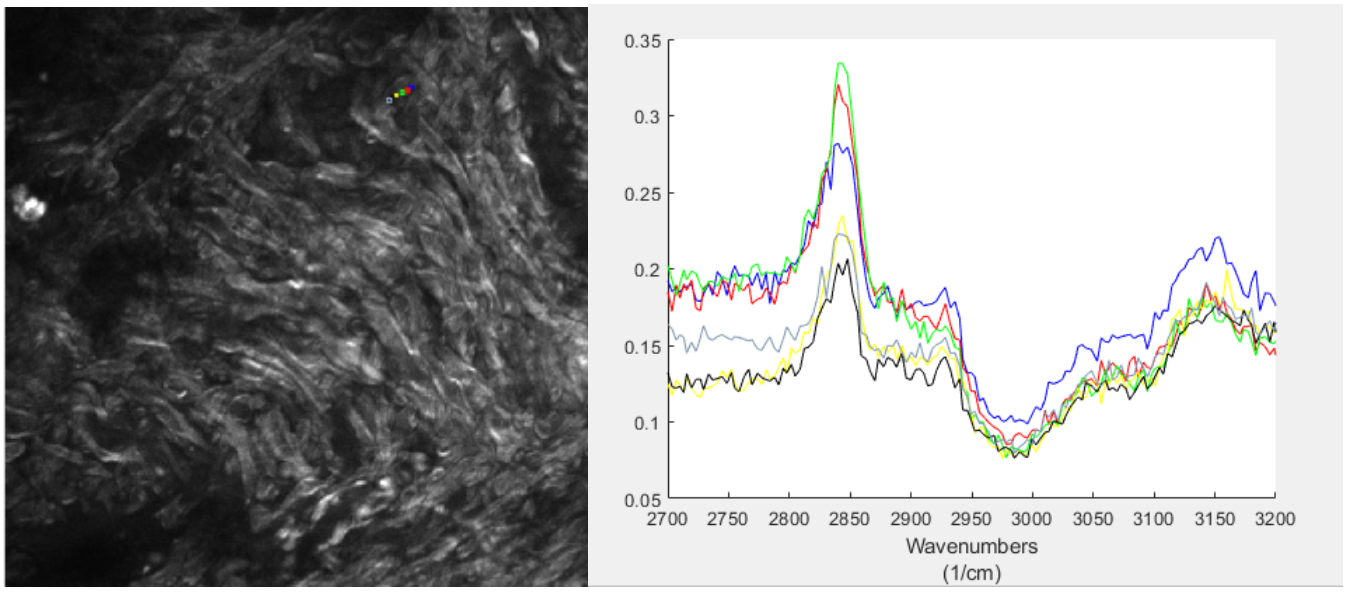

(a) *(b)*

Figure 5.1: a) A CARS image of brain matter, 5 pixel areas are selected in the top right. b) A spectral graph of the selected areas. The y-scale shows the intensity in arbitrary units.

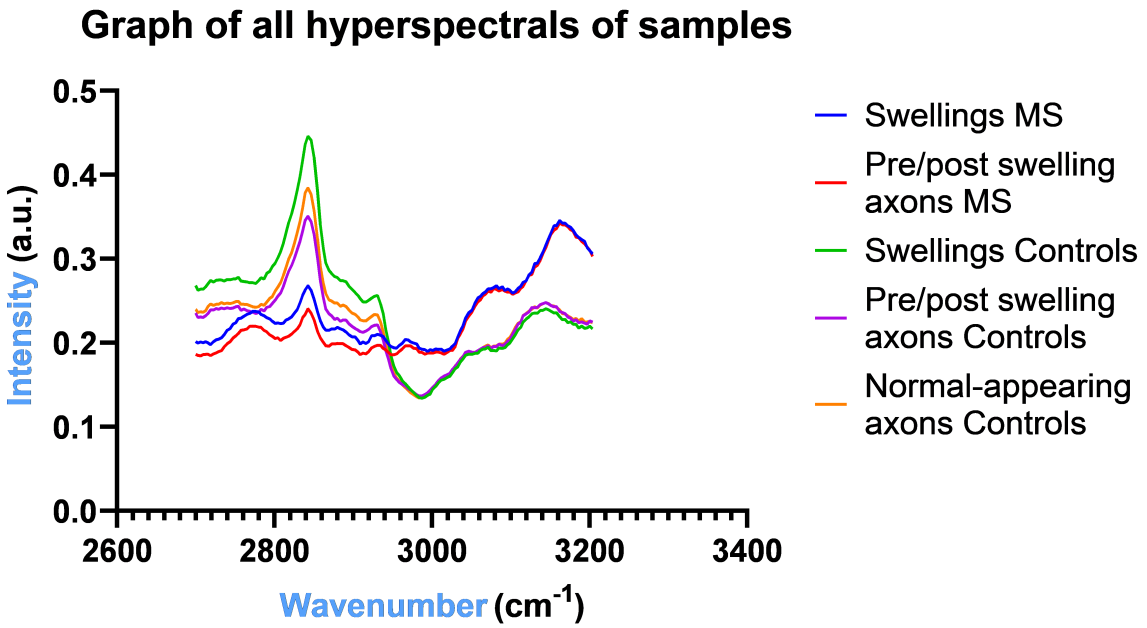

Figure 5.2: A hyperspectral of all samples grouped together. Notice the peak at the 2848 cm^{-1} wavenumber corresponding to a $C - H_2$ bond.

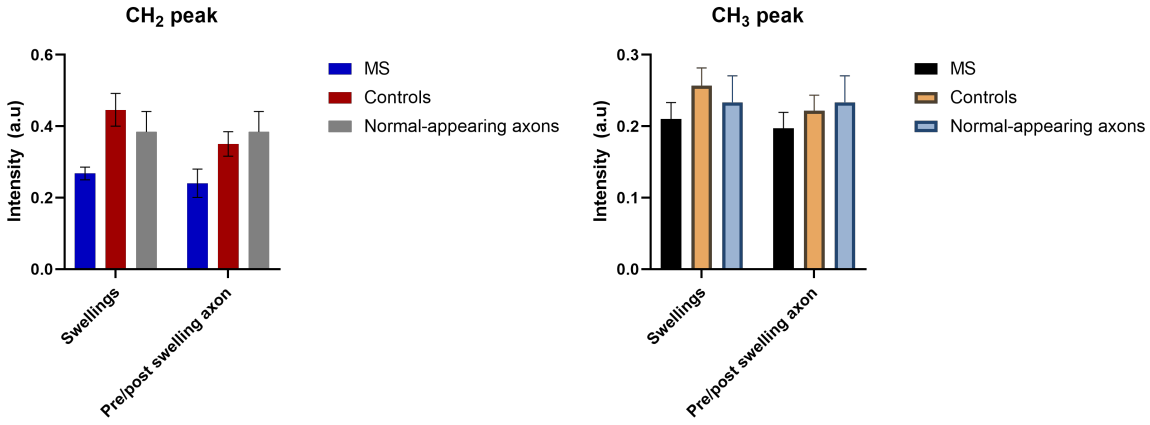

(a) *(b)*

Figure 5.3: a) A bar graph showing the intensity corresponding to the $C-H_2$ bond. b) A bar graph showing the intensity corresponding to the $C-H_3$ bond. Note that normal-appearing matter is the same in swelling and pre/post swelling, as they classify as both at the same time for easier comparison.

5.2 Statistical analaysis

To look even further into the data of the lipid bonds, a statistical analysis has been made using the GraphPad Prism^{TM} tool. Firstly it is interesting to look at how MS swellings compare to control sample swellings. The results are shown in table 5.1, with a total sample size of $n = 3$ for MS samples and $n = 5$ for control samples. The $C-H_2$ bond in swellings show a statistical significant difference between the MS swellings and the control swellings. The pre/post swellings do not show a significant change. This would mean that according to the results there is no difference in lipid bonds between MS samples and control samples in the region proximal and distal to the swelling. For the $C-H_3$ peak is no significant change found using these samples, which would suggest that $C-H_2$ is a better marker to look for to distinguish between MS and control samples.

Another region of interest is how swelled tissue compares to normal-appearing axons. In this case we are not trying to see if we are looking at MS tissue or not, we are trying to make a case for lower lipids leading to swelling. For normal-appearing axons had a sample size of $n = 4$. The results are shown in table 3.2 for the $C-H_2$ peak and in table 3.3 for $C-H_3$ peak. Only the $C-H_2$ peak shows a significant change in MS samples vs normal-appearing axons.

Statistical Welsh t-test of $C - H_2$ peak of MS versus Control				
Sample type	Below threshold?	t ratio	df	Adjusted P Value
Swellings	Yes	3,614	5,047	0,029903
Pre/post swelling axon	No	2,099	4,744	0,092917

Statistical Welsh t-test of $C - H_3$ peak of MS versus Control				
Sample type	Below threshold?	t ratio	df	Adjusted P Value
Swellings	No	1,362	5,628	0,399671
Pre/post swelling axon	No	0,7847	5,252	0,466532

Table 5.1: Top: A table showing statistical significant difference in $C - H_2$ peak of swellings in MS compared to control. Bottom: A table showing statistical significant difference in $C - H_3$ peak of swellings in MS compared to control

Statistical Welsh t-test of $C - H_2$ peak of MS versus Normal-appearing axon				
Sample type	Below threshold?	t ratio	df	Adjusted P Value
MS Swellings	Yes	3,485	4,713	0,038299
MS Pre/post swelling axon	Yes	2,944	3,877	0,043911

Statistical Welsh t-test of $C - H_3$ peak of Control versus Normal-appearing axon				
Sample type	Below threshold?	t ratio	df	Adjusted P Value
Control Swellings	No	1,139	6,391	0,503656
Control Pre/post swelling axon	No	0,7602	6,987	0,503656

Table 5.2: Top: A table showing statistical significant difference in $C - H_2$ peak of MS tissue compared to Normal-appearing axon. Bottom: A table showing statistical significant difference in $C - H_2$ peak of Control tissue compared to Normal-appearing axon

Statistical Welsh t-test of $C - H_3$ peak of MS versus Normal-appearing axon				
Sample type	Below threshold?	t ratio	df	Adjusted P Value
Swellings	No	0,7801	4,285	0,476171
Pre/post swelling axon	No	1,244	4,375	0,475839

Statistical Welsh t-test of $C - H_3$ peak of Control versus Normal-appearing axon				
Sample type	Below threshold?	t ratio	df	Adjusted P Value
Swellings	No	0,7416	6,857	0,73266
Pre/post swelling axon	No	0,4097	7	0,73266

Table 5.3: Top: A table showing statistical significant difference in $C - H_3$ peak of MS tissue compared to Normal-appearing axon. Bottom: A table showing statistical significant difference in $C - H_3$ peak of Control tissue compared to Normal-appearing axon

Chapter 6

Discussion

6.1 Changes in concentration of lipids

Looking at figure 5.1 we can see a peak around 2848 and a small peak around 2934 corresponding with their respective bindings. This gives us a good indication that we are indeed looking at lipids. The peak of water around 3140 is broad but can still be recognized. All swellings thus contain both lipids and water and are nicely comparable with one another. Figure 5.2 shows that a swelling produced by MS has a significant lower peak at 2848 than a normal axon corresponding to the $C-H_2$ bond. This supports the hypothesis that the lipid concentration changes due to the swelling. However, we can not conclude from this what happened to the lipids. It can either have been broken down or moved away. In any case it makes sense to say that lipid function would decrease. It seems that the water peak has increased as well, leading to a theory that the lipids have been replaced by water. It is also interesting that a swelling occurring in a control sample does not show these large changes. This does raise the question: Why does the lipid concentration decrease only in MS swellings? Furthermore, the study could not provide a significant difference in pre/post swellings between MS and control samples. However there *is* a significant change in lipid bonds between MS swellings and normal-appearing axons, which suggests that there is atleast a case for using lipid breakdown as a precursor to the creation of swellings. This supports the theory that neurotoxicity caused by higher Ca^{2+} uptake results in a higher chance of swelling.

6.2 Sample size

The sample size of the MS tissues and control tissues used during the study were quite small. This has an impact on the statistical analysis. The results this far show great potency and thus would require more testing with a larger sample size. MS can show signs of remission and relapsing and thus the sample size could vary wildly in progressive state of the disease. The only information that was known was whether

the tissue contained MS affected tissue or not. Therefore there was no correction or otherwise altered method in treating samples for different stages of MS. It could be that MS shows different signs of lipid breakdown in different stages of its development.

6.3 Imaging difficulties

The intensity during a hyperspectral is quite high, due to the nature of non-linear optics. Samples are scanned throughout a time window around the 25 minute mark. In this long time the sample will heat up and this can influence the electronic landscape. Multiple times the samples have been burned during measurements, thus requiring to lower the input power of the beam. This results in a lower CARS signal. An attempt at lower magnification was done to circumvent this but as said before, the regions of swellings are quite small and require a higher magnification to spot.

Another problem lies within the alignment of the stokes beam with the pump beam. Previous studies [12] done with the setup have shown that the intensity is strongest in the center of the scanning zone and decreases in strength towards the borders, with a factor up to ten percent. The swellings have therefore been centered in the scanning box for a fairer comparison between the samples, but this is still not optimal.

Chapter 7

Conclusions

7.1 Conclusions

The research question that this paper aimed to answer was: How does the concentration of lipids in myeline damaged by Multiple Sclerosis change after the swelling of an axon?"

The study succeeded in imaging a sample using CARS and acquiring a spectral graph of 8 total samples, containing the specific lipid bonds.The study revealed that the concentration in MS swellings are significantly lower ($P \approx 0.038$) compared to a healthy normal-appearing axon. This reduction is also significantly lower when comparing MS swellings to control swellings ($P \approx 0.030$).

These results thus provides support for using lipid breakdown as a marker towards swelling caused by MS, making a "inside-out" theory more plausible. The marker of choice should be focused around the $C - H_2$ bond.

Chapter 8

Recommendations & Outlook

This chapter contains some possible improvements concerning the CARS setup and a thorough explanation of a spontaneous Raman setup. A great deal of research time has gone into this setup, but due to time constraints it was not finished. Nevertheless, it can provide a good guideline as to how such a setup may help in acquiring new data.

8.1 Imaging improvements

Not all the samples were scanned at the same magnification. This results in a different quality of swelling selection. It was easier to identify swellings in images with a 62 times magnification compared to the normal 60 times. We have not looked at how the magnification influences the signal. For better comparison it is thus highly adviced to take all images at the same magnification, or make a magnification/intensity profile for calibration purposes.

Another way to improve the signal is to tune the voltage/gain of the PMT. For this research it has been set to a single value, but more signal can be acquired (and easily compensated for) using a higher voltage/gain. And while the PMT does vary its output compared to the wavelength, as long as all measurements are done using the same setup all images can still be compared.

8.2 Spontaneous Raman Setup

In Chapter 2 we explained Raman theory and how it is able to measure vibrations in bindings. In this section we provide a setup for spontaneous Raman, which is built-in the original CARS setup. The big advantage that spontaneous Raman brings is the eradication of the non-resonant background noise. This comes with a downside; spontaneous Raman has a very low acquisition signal. This makes CARS an excellent tool to scout for swellings, after which we can identify a position on which we can scan using the spontaneous Raman. As the intensity of the Raman signal depends linearly

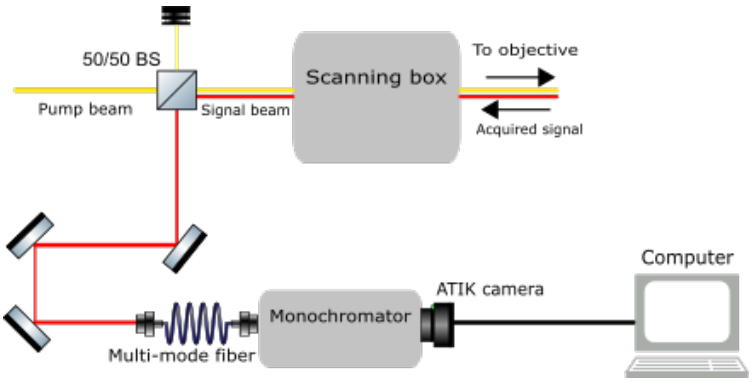

Figure 8.1: Setup of acquiring a spontaneous Raman signal

on the intensity of the incoming laser, we would like to let this laser be as high in intensity as possible. Using equation 2.1 we thus want to use the highest frequency possible. In the current setup, this is around the 2600 wavenumber which corresponds to 776 nm excitation wavelength. It is possible to tune the OPO even lower. We can not go too low though, as fluorescence will show up in the lower wavelength. With multiple scans we can remedy this, as fluorescence is based on absorption and thus only occurs at certain frequencies, while Raman uses virtual states and occurs at every frequency. Thus Raman will shift accordingly and fluorescence will stay fixed in a hyperspectral scan.

Figure 8.1 gives an outline as to how this setup can be realized. Because the setup uses an epi-detection method, we can use this channel for our benefit. Assuming that the signal does not spatially distort on the way back (the pathway back is identical to the pathway in), we can direct this signal towards a new detection mechanism. To create a new pathway out for the signal we use a 50/50 beamsplitter. This does have a big impact on the incoming light, which is now halved. And the acquired signal going back also is halved, resulting in a 75% reduction of intensity. Add on to that the multiple reduction factors of the objective, microscope and efficiency of the detector, and we will barely have any signal left. It is thus of the utmost importance that the intensity going in is as high as possible, and the components of the highest efficiency. The signal beam is then guided (with silver mirrors) towards another objective, which focuses the beam onto a fiber. The signal will also contain the chosen excitation frequency so this needs to be filtered out as well. A choice between single-mode and multi-mode fiber here can make a large difference. Multi-mode fibers can couple in a large amount of light, but also has more trouble focusing on the detector compared to a single-mode fiber. The fiber is connected to a monochromator (Cornerstone), which allows us to spectrally seperate the signal onto a charge coupled device (CCD). The detector of choice here is an ATIK camera.

Due to time constraints the setup was not fully worked out. The multi-mode fiber

Figure 8.2: Cover page of Annals of Neurology Volume 89, issue 4.

proved to be difficult to focus into the monochromator. A single-mode fiber proved to be workable but the amount of photon-loss was too high to be able to make a measurement. Also the coupling of the monochromator to the ATIK camera had alignment issues, losing yet more photons in the process.

8.3 Outlook

This research was conducted in 2019, and thus three years have past since the data was used for the MS research in Amsterdam. In 2021 the researchers have published their paper on blisters in MS tissue [3] and it has some promising results. The paper has been admitted to the Annals of Neurology and was the cover of Volume 89, issue 4. Results of this study has been used to provide support for the "inside-out" theory. Numerous other measurements have been made and the proposed pathway (figure 2.5) was the result of the combined efforts.

The paper looked intensively at the many other effects of higher Ca^{2+} uptake of the myeline. The citrullination and hydrolysis of MAG concentrations have been compared in the same way that this paper has compared the lipid concentrations.

Bibliography

[1] P. Browne, D. Chandraratna, C. Angood, H. Tremlett, C. Baker, B. V. Taylor, and A. J. Thompson, "Atlas of multiple sclerosis 2013: A growing global problem with widespread inequity," *Neurology*, vol. 83, no. 11, pp. 1022–1024, 2014. [Online]. Available: https://n.neurology.org/content/83/11/1022

[2] R. Yang, N. Xi, C. K. M. Fung, K. Seiffert-Sinha, K. W. C. Lai, and A. A. Sinha, "The emergence of afm applications to cell biology: How new technologies are facilitating investigation of human cells in health and disease at the nanoscale," *Journal of nanoscience letters*, vol. 1‘, no. 2, pp. 87–101, 2011, 24416719[pmid]. [Online]. Available: https://www.ncbi.nlm.nih.gov/pubmed/24416719

[3] A. Luchicchi, B. Hart, I. Frigerio, A.-M. van Dam, L. Perna, H. L. Offerhaus, P. K. Stys, G. J. Schenk, and J. J. G. Geurts, "Axon-myelin unit blistering as early event in MS normal appearing white matter," *Ann. Neurol.*, vol. 89, no. 4, pp. 711–725, Apr. 2021.

[4] C. C. Moura, R. S. Tare, R. O. C. Oreffo, and S. Mahajan, "Raman spectroscopy and coherent anti-stokes raman scattering imaging: prospective tools for monitoring skeletal cells and skeletal regeneration," *Journal of The Royal Society Interface*, vol. 13, no. 118, p. 20160182, May 2016. [Online]. Available: https://doi.org/10.1098/rsif.2016.0182

[5] E. Smith and G. Dent, *Modern Raman Spectroscopy: A Practical Approach*. Wiley, 2005.

[6] R. Rubin, D. S. Strayer, and E. Rubin, *Rubin's Pathology: Clinicopathologic Foundations of Medicine, Sixth Edition*. Lippincott Williams & Wilkins, 2012, pp. 1335 – 1337.

[7] W. F. Boron and E. L. Boulpaep, *Medical Physiology, Second Edition*. Saunders, 2009, pp. 320 – 322.

[8] P. Kumar and M. Clark, *Clinical Medicine, Seventh Edition*. Saunders, 2009, pp. 1151 – 1153.

[9] J. D. Haines, M. Inglese, and P. Casaccia, "Axonal damage in multiple sclerosis," *The Mount Sinai journal of medicine, New York*, vol. 78, no. 2, pp. 231–243, 2011, 21425267[pmid]. [Online]. Available: https://www.ncbi.nlm.nih.gov/pubmed/21425267

[10] "Fluorodish cell cultures," https://www.wpiinc.com/cell-and-tissue/cell-and-tissue-accessories/fluorodish-cell-cultures, 2018, accessed on 19-8-2019.

[11] L. Squire, D. Berg, F. E. Bloom, S. Du Lac, A. Ghosh, and N. C. Spitzer, *Fundamental neuroscience*. Academic Press, 2012.

[12] R. Jansen, "Nonlinear multimodal microscopy for ex-vivo breast cancer delineation," 2019.